PHOTONICS Research

Fabrication and near-infrared optical responses of 2D periodical Au/ITO nanocomposite arrays

Zhengyuan Bai,[1,2,3] Guiju Tao,[4,6] Yuanxin Li,[1,3] Jin He,[5] Kangpeng Wang,[2] Gaozhong Wang,[2] Xiongwei Jiang,[1] Jun Wang,[1] Werner Blau,[2] and Long Zhang[1,*]

[1]Key Laboratory of Materials for High Power Laser, Shanghai Institute of Optics and Fine Mechanics, Chinese Academy of Sciences, Shanghai 201800, China
[2]School of Physics and the Centre for Research on Adaptive Nanostructures and Nanodevices (CRANN), Trinity College Dublin, Dublin 2, Ireland
[3]University of Chinese Academy of Sciences, Beijing 100039, China
[4]Shanghai Research Institute of Petrochemical Technology, SINOPEC, Shanghai 201208, China
[5]Institute of Chemistry, the Hebrew University of Jerusalem, Jerusalem 91904, Israel
[6]e-mail: gjtao@siom.ac.cn
*Corresponding author: lzhang@siom.ac.cn

Received 8 March 2017; revised 26 April 2017; accepted 29 April 2017; posted 4 May 2017 (Doc. ID 290311); published 6 June 2017

Two-dimensional (2D) periodical Au and indium tin oxide (ITO) nanocomposite arrays have been fabricated based on a self-assembled nanosphere lithography technique. A button-shaped Au nanoparticle was formed on each hollow hemisphere-shaped ITO shell. Importantly, the underlying formation mechanism during the thermal treatment has been thoroughly explored by comparing structures resulting from different deposition conditions in detail. Compared to the Au nanoparticle arrays without ITO shells, the Au/ITO nanocomposite arrays showed a stronger localized surface plasmon resonance effect and higher absorption in the near-infrared (NIR) region, benefiting from the free-electron interaction enhancement between Au and ITO. The nonlinear optical properties were investigated using a modified femtosecond intensity-scan system, and the results demonstrated Au/ITO nanocomposite arrays with a remarkable two-photon absorption saturation effect for femtosecond pulses at 1030 nm. The versatile NIR optical responses indicate the great potential of the elaborately prepared 2D periodical Au/ITO nanocomposite arrays in many applications such as solar cells, photocatalysis, and novel nano optoelectronic devices.

OCIS codes: (190.4400) Nonlinear optics, materials; (230.4000) Microstructure fabrication; (160.4236) Nanomaterials.

https://doi.org/10.1364/PRJ.5.000280

1. INTRODUCTION

Ordered noble metal nanostructured arrays have attracted much attention due to their unique optical properties, which have shown promising application in a variety of fields, such as surface-enhanced Raman scattering (SERS) active substrates [1], solar cells [2], optoelectronic as well as plasmonic devices [3], and metamaterial absorbers [4]. As a typical noble metal material, Au nanostructured arrays have been widely studied and have become promising candidates in these areas. It is well known that the optical properties of Au nanostructured arrays depend directly on their size, shape, composition, and the surrounding environment corresponding to their localized surface plasmon resonance (LSPR) [5,6].

Up to now, various efficient methods, including lithography techniques and the template-based techniques [7], have been developed to fabricate periodical metal nanostructures and effectively control the space of arranged array structures. However, the main drawback of the lithography techniques (such as photolithography [8] and electron beam lithography [9]) lies in their high cost and low sample throughput. In the last decade, much attention has been focused on the template-based methods, which have proven to be simple, effective, and low cost. For instance, the nanosphere self-assembling template technique, which is known as self-assembled nanosphere lithography (NSL) [10], demonstrates a low-cost, high-throughput, and efficient method for the fabrication of periodic metallic nanostructures. By using the NSL techniques combined with subsequent processes, Li *et al.* proposed a facile strategy to prepare a variety of two-dimensional (2D) ordered Au nano arrays, e.g., nanoparticle arrays, nanoring arrays, and nanobowl arrays [11]. Yan *et al.* fabricated an Au-coated polystyrene nanosphere array with tunable optical properties by controlling the nanosphere gaps [12]. Wang *et al.* prepared a gold quasi rod-shaped nanoparticle-built hierarchically nanostructured pore

array via clean electrodeposition on a polystyrene nanosphere colloidal monolayer [13]. These structures fabricated by the NSL technique have presented different properties and potential applications. However, most studies have focused on the fabrication of various Au hierarchical nanostructures; it is still a big challenge to achieve controllable fabrication of ordered Au composite nanostructures with a uniform size.

Among a variety of transparent conducting materials, indium tin oxide (ITO) is the most widely used due to high optical transmittance and conductive properties, as well as its excellent adhesion properties to substrates [14]. Interest in assembling gold nanoparticles on ITO substrates has increased in recent years as the resulting interfaces have shown interesting optical properties. Szunerits *et al.* prepared Au island films on ITO substrates for localized surface plasmon sensing [15]. Duan *et al.* fabricated an ordered Au particle array with hierarchical surface roughness on an ITO substrate for SERS [16]. Therefore, it is of particular interest for the fabrication of Au and ITO composite nanostructures.

Herein, an Au and ITO nanocomposite array (referred to as Au/ITO-NA) has been fabricated simply by the NSL technique combined with an annealing treatment. This hybrid nanoantenna, which can be efficiently produced without using nanolithography techniques, is composed of hexagonally packed arrays of hollow hemisphere-shaped ITO shells, with one button-shaped Au nanoparticle on the top of each ITO shell. Importantly, the formation mechanism of this 2D NA has been studied by comparing the structures resulting from different depositions in detail. Moreover, this fabricated Au/ITO-NA exhibits excellent optical properties. Ultraviolet (UV)–visible–near-infrared (NIR) spectra have shown that this NA has a strong broadband optical extinction and enhanced absorption in the NIR due to the combined effects of the LSPR of Au nanoparticles and the free-electron interaction on Au/ITO interfaces. The Au/ITO-NA also exhibits a remarkable two-photon absorption (TPA) saturation effect for femtosecond (fs) pulses at 1030 nm, with a significant TPA coefficient of $(4.40 \pm 0.19) \times 10^2$ cm/GW. Therefore, it is believed that the proposed Au/ITO-NA with prominent versatile NIR optical responses would be promising in optical applications such as solar cells, photocatalysis, and novel nano optoelectronic devices.

2. EXPERIMENT

A. Materials

Monodispersed polystyrene spheres (PSs) (600 nm) in an aqueous suspension (2.5 wt. %) were purchased from Huge Biotechnol. Co., Ltd. (China). Quartz glass slides (50 mm × 30 mm × 1 mm) were used as substrate, and were ultrasonically cleaned in deionized water, acetone, ethanol, and deionized water for 30 min, and then dried with nitrogen gas before use. Triple deionized water was prepared from a Milli-*Q* water purification system (Shanghai Yarong Co., Ltd). The ITO target (purity, 99.99%) with a mass ratio between In_2O_3 and SnO_2 of 9:1 was purchased from Hefei Kejing Co., Ltd. All the reagents were of analytical-grade purity and were used directly without further purification.

B. Preparation of PS Colloidal Monolayer Template

The preparation process of the PS colloidal monolayer template is described in Figs. 1(a)–1(c). First, the substrate was exposed

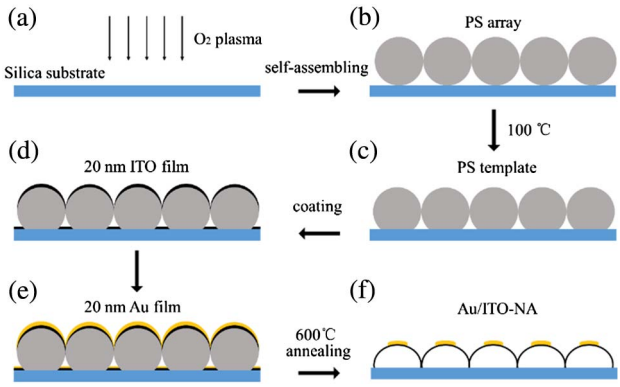

Fig. 1. Scheme of the Au/ITO-NA fabrication process.

to an oxygen gas plasma in the plasma cleaner (Shenzhen Dongxin High-Tech Co., Ltd.) with a power of 45 W for 180 s to enhance its hydrophily. Second, PSs were self-assembled into a 2D hexagonal and closely packed array by the air–liquid interface method [17]. In detail, the suspension of monodisperse PSs and ethanol was mixed together with a volume ratio of 1 to 2 and ultrasonically vibrated for 30 min. After the quartz substrate was placed horizontally, 600 μL deionized water was poured over it and then spread rapidly to form a water film. About 90 μL of the homogeneously mixed PS suspension was poured onto the water surface at one end of the substrate, and the PSs would spread over the water surface in several minutes. Then a monolayer colloidal crystal was formed at the air/liquid interface. After the solvent was evaporated completely, the self-assembled monolayer PSs were left on the substrate. Finally, a large area of colloidal monolayer template was formed after it was heated at 100 °C for 10 min in an oven to form a firm connection between the PSs and the substrate.

C. Fabrication of Au/ITO NA

The prepared PS colloidal monolayer template was first coated with 20 nm ITO film using the pulsed laser deposition method [18] with a 248 nm KrF excimer laser. Second, an Au film of the same thickness was coated onto the sample using the magnetic sputtering method. At last, the Au/ITO-NA was obtained after being annealed in a resistance furnace at 600 °C for 120 min with a heating rate of 5 °C/min and cooled naturally. The scheme of the above fabrication process is shown in Figs. 1(d)–1(f).

As mentioned above, we have produced the hybrid nanoantennas by a novel (to our knowledge) method without using nanolithography techniques. For comparison, different Au and ITO nanostructures have also been fabricated: (1) single ITO shell arrays with ITO film thickness of 15 nm (called ITO-15) and 20 nm (called ITO-20); (2) Au/ITO nanocomposites with 10 nm Au film (referred to as Au-10/ITO-20) and 30 nm Au film (referred to as Au-30/ITO-20); (3) 20 nm Au film deposited directly on the PS colloidal monolayer template (referred to as Au-20-NPA); (4) 20 nm Au film deposited directly on the substrate (referred to as Au-20-NPs). All the above samples were annealed under the same conditions as described above.

D. Characterization

The morphologies of all the prepared samples were characterized using a field emission scanning electron microscope (FESEM, Zeiss Auriga) and an atomic force microscope (AFM, Veeco Dimension 3100) to clearly show its three-dimensional topography. The proportion of Au and ITO in Au/ITO-NA was analyzed by an energy dispersive spectrometer. The spectral analysis of the sample was carried out using a LAMBDA 1050 UV/visible/NIR spectrometer along with a 150 mm integrating sphere (PerkinElmer, Inc., Shelton, Connecticut, USA).

3. RESULTS AND DISCUSSION

A large-area (more than 2 cm × 2 cm) periodical Au/ITO-NA was fabricated on the quartz glass substrate, with both Au and ITO films of 20 nm used for the deposition process. Figure 2(a) is a photograph of our fabricated sample. It can be seen that most of the quartz glass substrate is covered with the quite uniform Au/ITO nanocomposite film (the nonuniform area on the right side of the substrate resulted from the Au/ITO nanostructure being formed with no template). Typical FESEM images of the sample are shown in Fig. 2(b), indicating the uniformly distributed Au/ITO-NA. From the high-magnification scanning electron microscope (SEM) image of the front part [Fig. 2(d)] and the reversed part [Fig. 2(e)] of our sample, it can be observed that the Au/ITO-NA has a hexagonally packed array of hollow hemisphere-shaped ITO semi-shells, on each of which is a button-shaped Au nanoparticle. The central distance of the neighboring units is 600 nm, showing a nice template-replica process. The longitudinal profile of the sample can be obtained from the AFM result, as shown in Fig. 2(c). Along the blue dashed line, the first Au particle is absent, and thus it can be estimated that the average height of the Au nanoparticles is about 35 nm, which is a key parameter for our later nonlinear optical coefficient calculations. Energy dispersive spectrometry (EDS) was performed for the component analysis of our sample [Fig. 2(f)]. It is clear that our material contains Au, In, and Sn elements. Moreover, the EDS 2D mappings shown in the insert of Fig. 2(f) also show the hexagonally packed Au/ITO-NA more clearly. Therefore, a facile method by NSL with a subsequent annealing treatment has been successfully demonstrated for fabricating a large area of high-quality Au/ITO-NA structure.

During the annealing process, the evolution of the nanocomposite structures can be divided into two main processes [19]. On one hand, PS polymer templates were removed completely due to thermal decomposition, leaving the ITO shell of a hollow hemisphere shape. On the other hand, the Au film at the top layer shrank and finally evolved into button-shaped nanoparticles on the ITO shells. ITO film can remain stable over time, benefiting from its higher melt point [20]. Therefore, in order to optimize the deposition parameters for the as-designed composite structure, samples with different thicknesses of both Au and ITO films were fabricated. First, to get the optimized ITO thickness, samples with only ITO film were fabricated, the thickness of which was of 15 or 20 nm. As shown in Fig. 3(a), when the thickness of the ITO film was 15 nm (ITO-15), collapsed and even broken hollow hemisphere-shaped ITO shells were obtained after the annealing process, indicating that the ITO film was too thin to keep

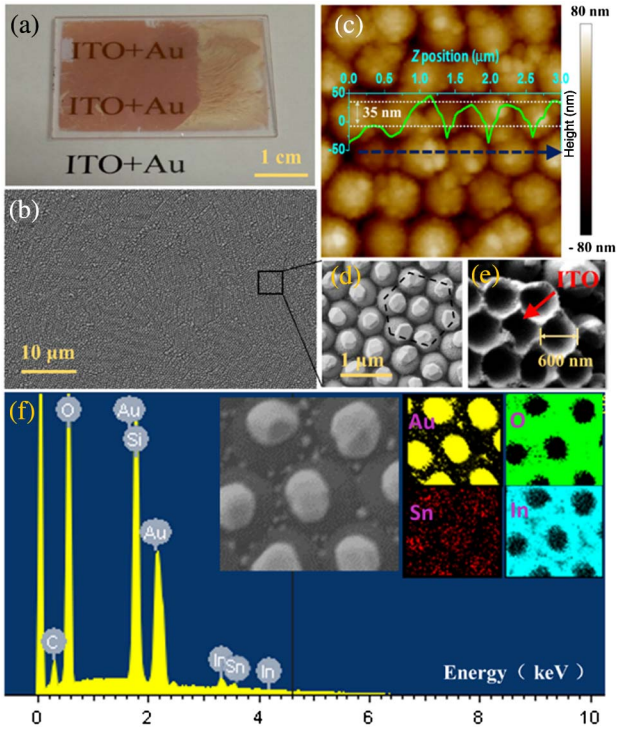

Fig. 2. (a) Digital photograph and (b) FESEM images of the Au/ITO-NA; (c) AFM topography of the sample and 2D longitudinal profile along the blue dashed line; high magnification SEM image of the (d) front and (e) back part of the Au/ITO-NA; (f) EDS results of the sample (inset: EDS 2D mapping of different elements in the Au/ITO-NA).

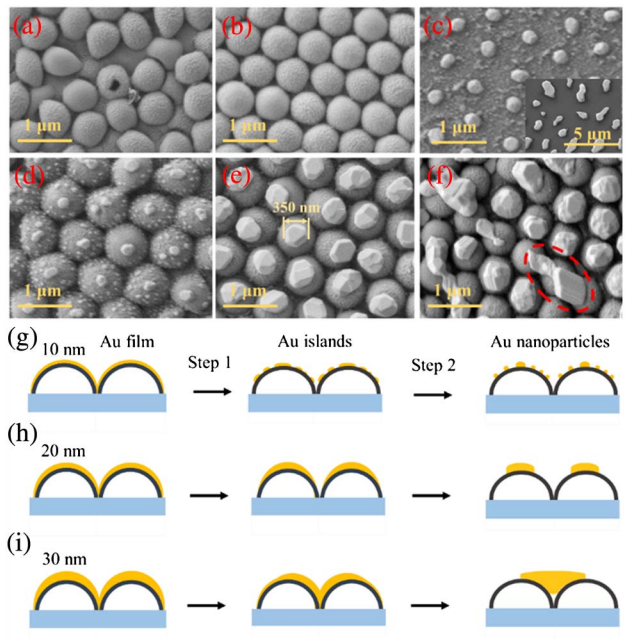

Fig. 3. SEM images of (a) ITO-15, (b) ITO-20, (c) Au-20-NPA (inset: Au-20-NPs), (d) Au-10/ITO-20, (e) Au/ITO-NA, and (f) Au-30/ITO-20; formation mechanism schemes of (g) Au-10/ITO-20, (h) Au/ITO-NA, and (i) Au-30/ITO-20.

its initial shell structure without the support of the PS template. However, when the thickness of the ITO film was increased to 20 nm (ITO-20), the stable hollow hemisphere-shaped ITO shell arrays could be integratively formed with hardly any defect, as shown in Fig. 3(b). There is no doubt that the thicker the ITO film is, the more stable the ITO nanostructure will be. However, for a better optical transmission property of the NA, a deposition thickness of 20 nm was chosen for our Au/ITO-NA design.

Second, Au films with thicknesses of 10, 20, and 30 nm were deposited on the 20 nm ITO film, followed by the same annealing process. Figure 3(d) is the SEM image of the sample deposited with 10 nm Au film (Au-10/ITO-20); it can be seen that the Au film has transformed into independent Au particles on each hollow hemisphere-shaped ITO shell, with a bigger one on the top surrounded by plenty of smaller ones. However, when the thickness of the Au film is increased to 20 nm, an ideal Au/ITO-NA structure with only one button-shaped Au particle on the top of each ITO shell is formed, as shown in Fig. 3(e). Nevertheless, as the thickness of the Au film is further increased to 30 nm (Au-30/ITO-20), aggregation of part Au particles on adjacent ITO shells will take place, as shown in Fig. 3(f). Based on the above results, it is indicated that the proper thicknesses of ITO and Au films are both key issues for the successful fabrication of the Au/ITO-NA.

More significantly, the underlying mechanism of different nanocomposite structures with Au thicknesses of 10, 20, and 30 nm should be demonstrated clearly. According to the theoretical studies on the dewetting of metallic thin films during heat treatment, the dewetting process is driven by surface and strain minimization [21]. As explained by the classical nucleation and growth theory, dewetting of metallic thin films starts with the formation of voids, which can take place at the grain boundaries [22], the film–substrate interface [23], and especially in areas of high local stress [24]. Subsequently, the formed voids grow larger, leading to the breaking up of continuous film into droplets or islands [25]. As for our sample with an Au film of 20 nm, voids first emerge at the edge of each ITO shell due to local stresses and then make the continuous gold film separate into discrete islands. These isolated gold islands on the ITO shells undergo the dewetting process independently, which finally leads to the formation of our ideal Au/ITO-NA structure [scheme in Fig. 3(g)]. However, for a thinner (10 nm) or thicker (30 nm) Au film, the dewetting processes are quite different. As for the Au-10/ITO-20, there are already numerous voids formed in the thin film during the sputtering process, which will behave as nuclei in annealing. Therefore, these small voids in the thin film will grow larger and larger during the annealing process, resulting in the discontinuous film being separated into a large number of isolated small-sized islands. Moreover, these small-sized islands will be difficult to move under the combined influence of gravity and the surface roughness of the ITO shells. Finally, each of the isolated islands will transform into dispersive Au particles under further annealing treatment [scheme in Fig. 3(h)]. Conversely, as for the Au-30/ITO-20, it is thick enough to prevent the growth of some voids at the edge of ITO shells. As the annealing proceeds, these voids disappear, accompanied by the aggregation of some connected Au islands on the adjacent ITO shells, which finally evolve into the larger-sized Au particles, as shown in the red dashed circle in Fig. 3(f) [scheme in Fig. 3(i)].

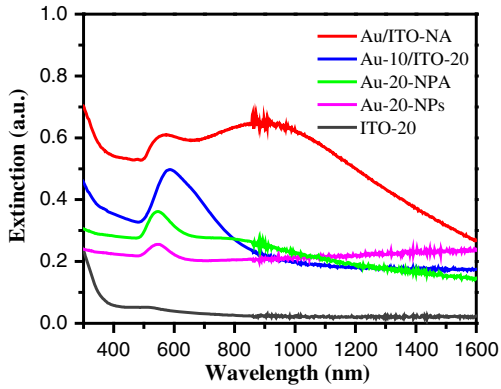

Fig. 4. Optical extinction spectra of all the prepared samples.

To investigate the optical properties of the as-prepared Au/ITO-NA, we first tested its linear optical spectra compared with those of other prepared samples from the visible to the NIR region. Figure 4 shows the optical extinction spectra of all the prepared samples. First, it can be observed from the gray line that there is little absorption or scattering in ITO-20, which indicates that ITO-20 with its minimal thickness could be regarded as a nearly transparent layer. Second, compared to Au-20-NPs with Au nanoparticles dispersed randomly (pink line), there is a stronger extinction peak in the Au-20-NPA (green line), which is ascribed to the stronger LSPR effect of Au-20-NPA due to the formation of the periodical Au nanoparticle arrays. However, compared to the Au-20-NPA and Au-20-NPs, an obviously enhanced and broadened LSPR peak can be observed for Au/ITO composites (Au/ITO-NA and Au-10/ITO-20). As for Au-10/ITO-20, it is clear to see that the extinction peak has been greatly enhanced and broadened with a redshift of the peak from 550 to 600 nm, which could result from the following possible factors. First, since ITO is a transparent free-electron conductor in the visible and near-IR region [26], the free-electron interaction between Au and ITO by optical excitation would be a key factor to enhance the LSPR strength of the Au nanoparticles. Second, since the regularly dispersed Au particles are formed on the ITO shell arrays, their modulated shape and size could be another reason for the enhancement and broadening of the LSPR effect. Moreover, the light-scattering of the Au particles could be enhanced by the structural modulation of the periodical template, which is also responsible for the redshift of the resonance peak.

As for Au/ITO-NA, in addition to the extinction peak near 600 nm, which is similar to Au-10/ITO-20, there is a stronger broadband peak near 900 nm, which would be of great potential in many applications such as SERS, optoelectronic devices, and solar cell areas. On one hand, as the average lateral dimension of the button-shaped Au nanoparticles on top of the ITO shells is about 350 nm [Fig. 3(e)], this strong resonance peak should correspond to the sized-dependent LSPR mode of the Au nanoparticles under TM mode stimulation of the incident

optical field [27]. Due to the larger interface area, the free-electron interaction region between ITO shells and Au nanoparticles will be much larger in Au/ITO-NA than that in Au-10/ITO-20. As a result, the LSPR strength of the Au particles can be enhanced greatly. On the other hand, according to the well-known Mie theory [28], the total Mie extinction is a sum of contributions from absorption and scattering components. It is well known that larger particles have a larger scattering cross section; considering the average size of the Au nanoparticles is over 300 nm, the light scattering in the NA should play a key role in the large light extinction. Therefore, to investigate the optical properties of the Au/ITO-NA more thoroughly, a 150 mm integrating sphere is employed for the further optical absorption and a scattering test.

Figure 5(a) shows the absolute value of the optical extinction, absorption, and scattering of the Au/ITO-NA. In the short wavelength band from 300 to 560 nm, it is observed that the optical absorption of the sample is more prominent, while in the longer waveband from 600 nm to the NIR region, the optical scattering becomes much greater than the absorption. It is indicated that the size-dependent optical scattering of the Au nanoparticles plays a dominant role in the strong LSPR effect in the NIR region. Nevertheless, it is easy to see the absorption enhancement of the Au/ITO-NA compared to that of the Au-20-NPA, as shown in Fig. 5(b). More importantly, there is a broad optical absorption band in the NIR region with a central peak near 1100 nm in Au/ITO-NA, which is absent in Au-20-NPA. This enhanced absorption peak should also be ascribed to the LSPR effect of the Au particles: when light is scattered by a metal nanoparticle, the electric field distributed on its surface can be enhanced by orders of magnitude [29],

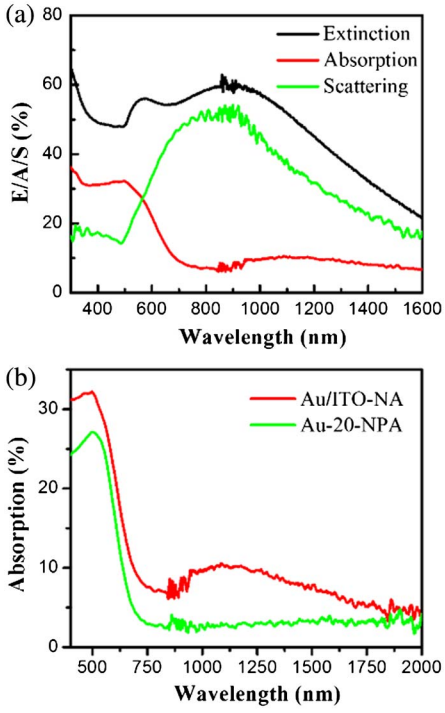

Fig. 5. (a) Extinction (E), absorption (A), and scattering (S) of the Au/ITO-NA; (b) comparison of the absolute absorbance of Au/ITO-NA and Au-20-NPA.

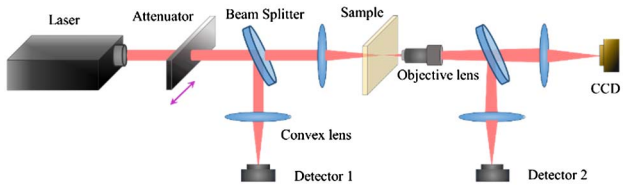

Fig. 6. Schematic diagram of the fs-I-scan system used for the nonlinear transmission/absorption experiment.

which then promotes the resonance absorption. At the same time, the strong free-electron interaction on the Au/ITO interface could contribute to the NIR absorption by enhancing the LSPR resonance of the Au particles. Moreover, the redshift of the absorption band compared to the LSPR peak should also be ascribed to the free-electron interaction between Au and ITO, which could change the plasmon frequency of Au nanoparticles [30].

It is widely known that Au nanoparticles can exhibit a nonlinear optical response several orders of magnitude larger than bulk metals due to its prominent SPR effects [31]. In this work, to further investigate the nonlinear optical properties of the Au/ITO-NA, a modified femtosecond intensity-scan system (fs-I-scan) [32,33] has been built up, as illustrated in Fig. 6. All experiments were performed by using 340 fs pulses from a mode-locked fiber laser operating at 1030 nm with a repetition rate of 1 kHz. The focus length of the convex lens is 10 cm, and an objective ($50\times$, N.A. $= 0.85$) is used to collect the signal after the sample. It should be noted that we selected several different points on the sample and repeated our measurement at least three times for each point to ensure the results are reliable. According to the experimental result shown in Fig. 7, the sample exhibits a typical TPA effect [34] as the normalized transmission reduces gradually with rising I_0, and tends to be stable when I_0 is above 110 GW/cm^2. According to the linear absorption spectrum of the Au/ITO-NA, as shown in Fig. 5(b), there is strong absorption (33%) at 515 nm, which is much greater than that at 1030 nm. Therefore, the sample shows a significant TPA effect, in which the free electron of the Au particles can absorb two photons simultaneously when excited by fs pulses at 1030 nm.

Based on the nonlinear optical theory, the attenuation of a light beam [$I(z)$] passing through an optical medium caused by TPA can be described as [35]

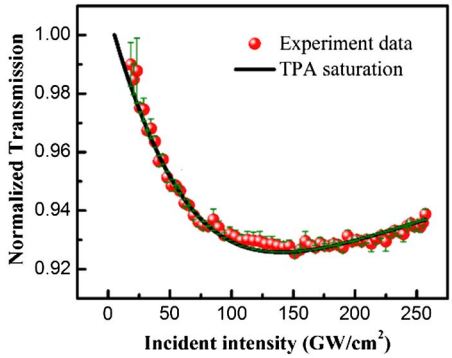

Fig. 7. TPA saturation effect of the Au/ITO-NA under the excitation of 340 fs, 1030 nm, and 1 kHz laser pulses.

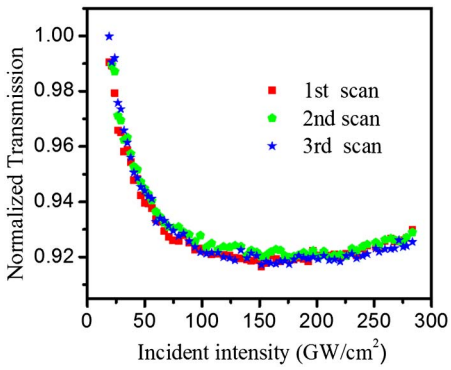

Fig. 8. TPA measurement results with repeated scan at the same point on the sample.

$$\frac{dI(z)}{dz} = -\alpha_0 I(z) - \beta(I) I^2(z), \tag{1}$$

where α_0 is the linear absorption coefficient derived from $T_0 = e^{-\alpha_0 \cdot L}$ [T_0 is the linear transmission ($T_0 = 1 - A - S$) and L is the thickness of the sample], $\beta(I)$ is the TPA coefficient, and z is the propagation distance in the sample. The change in β with incident intensity (I_0) can be expressed as [36]

$$\beta(I_0) = \frac{\beta_0}{1 + \left(\frac{I_0}{I_{s,\mathrm{TPA}}}\right)^2}, \tag{2}$$

where β_0 is the nonsaturation TPA coefficient and $I_{s,\mathrm{TPA}}$ is the TPA-induced saturable intensity of the sample. In our experiment, no clear nonlinear response from either the ITO shells or the quartz substrate was observed. Therefore, the contribution of $\beta(I_0)$ only originates from the Au nanoparticles. More important, according to the repeated measurement results at one point, the TPA signal was stable and no damage was observed, as shown in Fig. 8; thus it can be demonstrated that the Au/ITO-NA structure can keep a stable TPA response under high-power fs laser radiation. According to Eqs. (1) and (2), a well-fitted result from the experiment data can be obtained, as shown in Fig. 6. The corresponding TPA coefficient β_0 is $(4.40 \pm 0.19) \times 10^2$ cm/GW, and $I_{s,\mathrm{TPA}}$ is 113 GW/cm^2. The results have demonstrated that our Au/ITO-NA has an excellent nonlinear absorption property in the NIR region, which might have great potential for nonlinear nano optical devices.

4. CONCLUSIONS

In summary, an Au/ITO-NA with a button-shaped Au particle on each hemisphere-shaped ITO shell has been fabricated based on the combined methods of NSL and thermal decomposition, instead of using nanolithography techniques. Deposition thicknesses of the ITO and Au films are key issues for the successful fabrication of the Au/ITO-NA, and its underlying formation mechanism has been discussed. Moreover, the Au/ITO-NA shows an enhanced LSPR band in the NIR, which could benefit from the free-electron interaction between Au and ITO. An integrating sphere is also employed to help investigate its linear optical properties thoroughly. Compared to the Au nanoparticle array without an ITO shell, the Au/ITO-NA has shown a distinct absorption band near 1100 nm. The nonlinear optical response has demonstrated that the Au/ITO-NA shows a remarkable TPA effect for fs pulses at 1030 nm, with a TPA coefficient of $(4.40 \pm 0.19) \times 10^2$ cm/GW, which corresponds to the strong intrinsic absorption band of Au nanoparticles. Therefore, this NA structure with prominent optical properties may have great potential in NIR optical applications such as solar cells, photocatalysis, and novel nano optoelectronic devices.

Funding. National Natural Science Foundation of China (NSFC) (61308087, 61405224, 61522510, 61675217); Natural Science Foundation of Shanghai (16ZR1440300); China Scholarship Council (CSC); Science Foundation Ireland (SFI); Chinese Academy of Sciences (CAS) (XDB16030700; QYZDB-SSW-JSC041); Science and Technology Commission of Shanghai Municipality (STCSM) (17XD1403900).

Acknowledgment. Z. B. thanks Dr. Yingbo He of Peking University for his help and thanks the CSC for the financial support. W. B. thanks the SFI for the financial support. J. W. thanks the NSFC, the Strategic Priority Research Program of CAS, the Key Research Program of Frontier Science of CAS, and the STCSM Excellent Academic Leader of Shanghai program.

REFERENCES

1. S. Cataldo, J. Zhao, F. Neubrech, B. Frank, C. Zhang, P. V. Braun, and H. Giessen, "Hole-mask colloidal nanolithography for large-area low-cost metamaterials and antenna-assisted surface-enhanced infrared absorption substrates," ACS Nano **6**, 979–985 (2012).
2. P. C. Tseng, M. A. Tsai, P. Yu, and H. C. Kuo, "Antireflection and light trapping of subwavelength surface structures formed by colloidal lithography on thin film solar cells," Prog. Photovoltaics **20**, 135–142 (2012).
3. M. Ren, B. Jia, J. Y. Ou, E. Plum, J. Zhang, K. F. MacDonald, A. E. Nikolaenko, J. Xu, M. Gu, and N. I. Zheludev, "Nanostructured plasmonic medium for terahertz bandwidth all-optical switching," Adv. Mater. **23**, 5540–5544 (2011).
4. W. Li and J. Valentine, "Metamaterial perfect absorber based hot electron photodetection," Nano Lett. **14**, 3510–3514 (2014).
5. W. P. McConnell, J. P. Novak, L. C. Brousseau, R. R. Fuierer, R. C. Tenent, and D. L. Feldheim, "Electronic and optical properties of chemically modified metal nanoparticles and molecularly bridged nanoparticle arrays," J. Phys. Chem. B **104**, 8925–8930 (2000).
6. M. E. Stewart, C. R. Anderton, L. B. Thompson, J. Maria, S. K. Gray, J. A. Rogers, and R. G. Nuzzo, "Nanostructured plasmonic sensors," Chem. Rev. **108**, 494–521 (2008).
7. Y. Li, G. Duan, G. Liu, and W. Cai, "Physical processes-aided periodic micro/nanostructured arrays by colloidal template technique: fabrication and applications," Chem. Soc. Rev. **42**, 3614–3627 (2013).
8. A. Revzin, R. J. Russell, V. K. Yadavalli, W.-G. Koh, C. Deister, D. D. Hile, M. B. Mellott, and M. V. Pishko, "Fabrication of poly (ethylene glycol) hydrogel microstructures using photolithography," Langmuir **17**, 5440–5447 (2001).
9. C. Vieu, F. Carcenac, A. Pepin, Y. Chen, M. Mejias, A. Lebib, L. Manin-Ferlazzo, L. Couraud, and H. Launois, "Electron beam lithography: resolution limits and applications," Appl. Surf. Sci. **164**, 111–117 (2000).
10. C. L. Haynes and R. P. Van Duyne, "Nanosphere lithography: a versatile nanofabrication tool for studies of size-dependent nanoparticle optics," J. Phys. Chem. B **105**, 5599–5611 (2001).
11. Y. Li, W. Cai, and G. Duan, "Ordered micro/nanostructured arrays based on the monolayer colloidal crystals," Chem. Mater. **20**, 615–624 (2008).

12. W.-G. Yan, J.-W. Qi, Z.-B. Li, and J.-G. Tian, "Fabrication and optical properties of Au-coated polystyrene nanosphere arrays with controlled gaps," Plasmonics **9**, 565–571 (2014).
13. J. Wang, G. Duan, G. Liu, Y. Li, Z. Dai, H. Zhang, and W. Cai, "Gold quasi rod-shaped nanoparticle-built hierarchically micro/nanostructured pore array via clean electrodeposition on a colloidal monolayer and its structurally enhanced SERS performance," J. Mater. Chem. **21**, 8816–8821 (2011).
14. T. Minami, "Present status of transparent conducting oxide thin-film development for indium-tin-oxide (ITO) substitutes," Thin Solid Films **516**, 5822–5828 (2008).
15. S. Szunerits, V. G. Praig, M. Manesse, and R. Boukherroub, "Gold island films on indium tin oxide for localized surface plasmon sensing," Nanotechnology **19**, 195712 (2008).
16. G. Duan, W. Cai, Y. Luo, Y. Li, and Y. Lei, "Hierarchical surface rough ordered Au particle arrays and their surface enhanced Raman scattering," Appl. Phys. Lett. **89**, 181918 (2006).
17. Z. Dai, Y. Li, G. Duan, L. Jia, and W. Cai, "Phase diagram, design of monolayer binary colloidal crystals, and their fabrication based on ethanol-assisted self-assembly at the air/water interface," ACS Nano **6**, 6706–6716 (2012).
18. H. Kim, C. Gilmore, A. Pique, J. Horwitz, H. Mattoussi, H. Murata, Z. Kafafi, and D. Chrisey, "Electrical, optical, and structural properties of indium-tin–oxide thin films for organic light-emitting devices," J. Appl. Phys. **86**, 6451–6461 (1999).
19. W.-G. Yan, C.-L. Luo, J. Zhao, M.-L. Guo, Q. Ye, Z.-B. Li, and J.-G. Tian, "Fabrication of Au nanoparticle composite TiO_2 shell arrays by controlled decomposition of polymer particles," Superlattices Microstruct. **75**, 371–377 (2014).
20. K. Y. Kim and S. B. Park, "Preparation and property control of nano-sized indium tin oxide particle," Mater. Chem. Phys. **86**, 210–221 (2004).
21. D. T. Danielson, D. K. Sparacin, J. Michel, and L. C. Kimerling, "Surface-energy-driven dewetting theory of silicon-on-insulator agglomeration," J. Appl. Phys. **100**, 083507 (2006).
22. W. W. Mullins, "Theory of thermal grooving," J. Appl. Phys. **28**, 333–339 (1957).
23. D. Wang and P. Schaaf, "Thermal dewetting of thin Au films deposited onto line-patterned substrates," J. Mater. Sci. **47**, 1605–1608 (2012).
24. U. Smith, N. Kristensen, F. Ericson, and J. Å. Schweitz, "Local stress relaxation phenomena in thin aluminum films," J. Vac. Sci. Technol. A **9**, 2527–2535 (1991).
25. M. Dufay and O. Pierre-Louis, "Anisotropy and coarsening in the instability of solid dewetting fronts," Phys. Rev. Lett. **106**, 105506 (2011).
26. O. Mryasov and A. J. Freeman, "Electronic band structure of indium tin oxide and criteria for transparent conducting behavior," Phys. Rev. B **64**, 233111 (2001).
27. T. K. Sau, A. L. Rogach, F. Jäckel, T. A. Klar, and J. Feldmann, "Properties and applications of colloidal nonspherical noble metal nanoparticles," Adv. Mater. **22**, 1805–1825 (2010).
28. Q. Fu and W. Sun, "Mie theory for light scattering by a spherical particle in an absorbing medium," Appl. Opt. **40**, 1354–1361 (2001).
29. J. D. Jackson, *Classical Electrodynamics* (Wiley, 1999).
30. S. Franzen, C. Rhodes, M. Cerruti, R. W. Gerber, M. Losego, J.-P. Maria, and D. Aspnes, "Plasmonic phenomena in indium tin oxide and ITO-Au hybrid films," Opt. Lett. **34**, 2867–2869 (2009).
31. R. Philip, P. Chantharasupawong, H. Qian, R. Jin, and J. Thomas, "Evolution of nonlinear optical properties: from gold atomic clusters to plasmonic nanocrystals," Nano Lett. **12**, 4661–4667 (2012).
32. B. Taheri, H. Liu, B. Jassemnejad, D. Appling, R. C. Powell, and J. Song, "Intensity scan and two photon absorption and nonlinear refraction of C_{60} in toluene," Appl. Phys. Lett. **68**, 1317–1319 (1996).
33. Y. Li, N. Dong, S. Zhang, X. Zhang, Y. Feng, K. Wang, L. Zhang, and J. Wang, "Giant two-photon absorption in monolayer MoS_2," Laser Photon. Rev. **9**, 427–434 (2015).
34. G. Ramakrishna, O. Varnavski, J. Kim, D. Lee, and T. Goodson, "Quantum-sized gold clusters as efficient two-photon absorbers," J. Am. Chem. Soc. **130**, 5032–5033 (2008).
35. M. Sheik-Bahae, A. A. Said, T.-H. Wei, D. J. Hagan, and E. W. Van Stryland, "Sensitive measurement of optical nonlinearities using a single beam," IEEE J. Quantum Electron. **26**, 760–769 (1990).
36. R. Schroeder and B. Ullrich, "Absorption and subsequent emission saturation of two-photon excited materials: theory and experiment," Opt. Lett. **27**, 1285–1287 (2002).